Pis'ma v ZhETF, vol. 100, iss. 6, pp. 451 – 456

Temperature evolution of polar states in $GdMn_2O_5$ and $Gd_{0.8}Ce_{0.2}Mn_2O_5$

V. A. Sanina[1)], *E. I. Golovenchits, B. Kh. Khannanov, M. P. Scheglov, V. G. Zalesskii*

Ioffe Physical Technical Institute of the RAS, 194021 S.Petersburg, Russia

Submitted 20 August 2014

The polar order along the c axis is revealed in $GdMn_2O_5$ and $Gd_{0.8}Ce_{0.2}Mn_2O_5$ at $T \le T_{C1} \approx 160$ K for the first time. This polar order is induced by the charge disproportion in the 2D superstructures emerged due to phase separation. The dynamic state with restricted polar domains of different sizes is found at $T > T_{C1}$ which is typical of the diffuse ferroelectric phase transition. At the lowest temperatures ($T < 40$ K) two polar orders of different origins with perpendicular orientations (along the b- and c-axes) coexist. The 1D superlattices studied by us earlier in the set of RMn_2O_5 multiferroics are the charged domain walls which separate of these polar order domains.

DOI: 10.7868/S0370274X14180118

1. Introduction. Orthorhombic (space group ($Pbam$)) manganites RMn_2O_5 (R rare earth ion) are examples of multiferroics in which ferroelectricity occurs at the temperature similar to that of a special type of magnetic ordering and is driven by it [1–3]. These multiferroics are characterized by a strong magnetoelectric effect. The possibility to control electric (magnetic) properties by applying a magnetic (electric) field attracts considerable attention to these materials.

All ions in RMn_2O_5 (RMO) are in the layers perpendicular to the c-axis [4]. The unit cell of RMO contains a Mn^{3+} ion and a Mn^{4+} ion. Mn^{4+} ions occupy positions $z = 0.25$ c and $1 - z = 0.75$ c and Mn^{3+} ions are in positions $z = 0.5$ c; R^{3+} ions occupy positions $z = 0$ c. Thus, RMO multiferroics contain equal quantities of manganese ions with different valences and a distribution of these ions in the crystal (charge order) is the governing factor determining of RMO properties.

There are two various types of the charge orders in RMO. The first one results from a paired arrangement of the Mn^{3+} and Mn^{4+} ions along the b-axis. The mutual spin orientation of these ion pairs alternates, i.e., ferromagnetic pairs alternate with antiferromagnetic ones. A strong double exchange arises between the ferromagnetic Mn^{3+}–Mn^{4+} ion pairs [5]. A weaker indirect exchange is characteristic of the antiferromagnetic ion pairs. As a result of the exchange striction, distances between ferromagnetic and antiferromagnetic pairs change. This breaks the lattice centrosymmetricity and gives rise to the polarization along the b-axis at temperatures $T \le T_C \approx (30{-}35)$ K [6]. The second type of the charge ordering is caused by the phase separation which is typical of all manganites containing ions Mn^{3+} and Mn^{4+} [5, 7]. The phase separation leads to the formation of conducting ferromagnetic domains inside antiferromagnetic (paramagnetic) manganite matrix.

In $R_{1-x}Ce_xMn_2O_5$ (RCMO), Ce^{4+} ions substitute R^{3+} ions, thus forming excess electrons that recharge manganese ions in neighboring planes $z = 0.25$ c and $1 - z = 0.75$ c. The doping scheme is $R^{3+} = Ce^{4+} + \mathbf{e}$, $Mn^{4+} + \mathbf{e} \leftrightarrow Mn^{3+}$. Besides there is a probability that e_g electrons of some Mn^{3+} ions from layers with $z = 0.5$ c can tunnel to Mn^{4+} ions in layers with $z = 0.25$ c and $1 - z = 0.75$ c. Such process is bound to be in RMO and RCMO. Charge carriers and ferromagnetic Mn^{3+}–Mn^{4+} ion pairs appear in both these crystals but their concentrations are more high in RCMO. The detail studies of the high permittivity and magnetic states existed in $Eu_{0.8}Ce_{0.2}Mn_2O_5$ (ECMO) due to the phase separation and charge carrier self-organization were reported in [8, 9]. We believe that as it was in ECMO the phase separation in $Gd_{0.8}Ce_{0.2}Mn_2O_5$ (GCMO) leads to formation of the conducting ferromagnetic domains inside the layers perpendicular to the c-axis due to layered GMO crystal structure. These domains line up along the c-axis, thus forming 2D superstructures. These superstructures emerge at all temperatures but their states are temperature dependent. The superstructure period along the c-axis at room temperature in ECMO was found to be ≈ 700 Å [8, 9].

Charge carrier self-organization gives rise to a dynamic equilibrium superstructures state with a balance between attraction forces (double exchange, Jahn-Teller interaction for the Mn^{3+} ions) and Coulomb repulsion

[1)]e-mail: sanina@mail.ioffe.ru

of charge carriers [5, 7]. Note that the possibility of 2D phase separation was demonstrated for electron system using an electrostatic approach [10, 11].

In this paper the comparison study of both the initial GMO and doped GCMO single crystals is presented. Symmetries of GCMO and GMO at room temperature are similar, and their lattice parameters are close. The studies of the polarization, dielectric permittivity, conductivity, X-ray diffraction, and the influence of magnetic field on these parameters are reported.

2. Experimental data and analysis. The as-grown single crystals were in the form of 2–3 mm thick plates with areas of 3–5 mm^2. To measure conductivity, dielectric permittivity, and polarization, capacitors with a thickness of 0.5–1.5 mm and area of 3–4 mm^2 were used. Conductivity and capacitance were measured by a Good Will LCR-819 impedance meter in the frequency range 0.5–50 kHz at 5–350 K. The polarization was determined by integrating of the pyrocurrent (I_{pyro}) measured by electrometer Keitchly 6514 during sample heating with a constant temperature variation rate after the preliminary of it cooling in the polarized electric field switched off at the lowest temperature.

2.1. $GdMn_2O_5$. Among RMO, GMO (with $R = Gd$) is of special interest. Recently, an observation of the abnormally high polarization along the b-axis in GMO ($P_b = 0.36\,\mu C/cm^2$) was reported in [12]. The usual values of P_b in RMO are 0.03–0.05 μC/cm^2 [3]. X-ray magnetic scattering in off-resonance and at the Gd L_3-edge (resonance) conditions in GMO have shown that both magnetic subsystems (Mn and Gd) are highly interrelated and form a common order parameter. An incommensurate magnetic structure with wave vector $q = (0.49, 0, 0.18)$ arises in the temperature range $T_{N1} = 33\,K$ – $T_{N2} = 30\,K$. At $T_{N2} = 30\,K$ a lock-in transition into a commensurate magnetic phase with wave vector $q = (1/2, 0, 0)$ occurs which exist to the lowest temperatures. The polar order in GMO emerges at $T_C \leq T_{N2}$ [12]. Note that the antiferromagnetic resonance branch typical of the uniaxial antiferromagnetic collinear structure along the a axis was observed earlier for GMO at $T < 30\,K$. A spectrum attributed to the paramagnetic Gd subsystem was also observed [13, 14]. The unusual magnetic and polar states of GMO should be sought for in properties of the ground state $^8S_{7/2}$ of the Gd^{3+} ions with a large spin $S = 7/2$ which weakly interact with the lattice but cause the strong uniform Gd–Mn exchange. This exchange enhances the exchange striction and the polar order along the b-axis.

An abnormally high polarization in GMO along the b-axis (P_b) was confirmed by us (Fig. 1). Along with this, it was found that the maxima in I_{pyro} near 30 K in an absence of polarized field and after application of this field $E = \pm 2.7$ kV/cm were close in magnitude and of the same sign. This means that rigid polarization is formed in the high internal field and the usual 180-degree domain structure is not formed in GMO. We believe that P_b is formed in the periodically changed internal electric field caused by alternation of the ferromagnetic and antiferromagnrtic Mn^{3+} - Mn^{4+} ion pairs along the b-axis. The uniform polarized electric field may only decrease of that internal field.

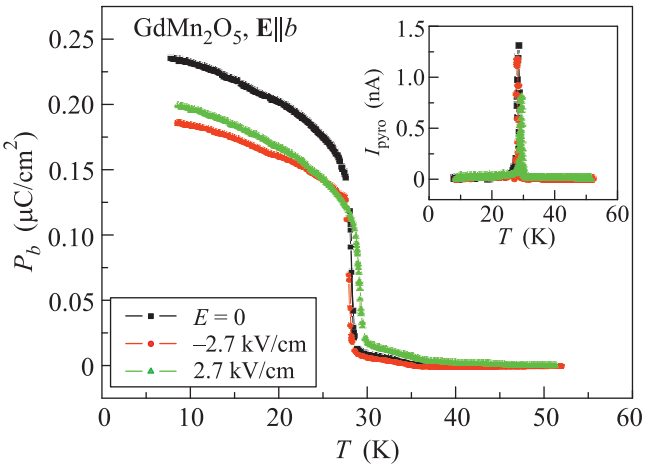

Fig. 1. Temperature dependence of P_b without preliminary applying of polarized electric field and after $E_b = \pm 2.7$ kV/cm application. Inset shows the same for $I_{\text{pyro}}(T)$

Fig. 2a shows the $I_{\text{pyro}}(T)$ and $P(T)$ dependences in GMO along the c-axis. It can be seen that P and I_{pyro} are two orders of magnitude lower than these parameters along the b-axis. However, they emerge at more high temperatures up to 160 K. Note that the P_c also occurs in the internal field. Preliminary application of the polarized electric field results in P_c reduction. One can see from Fig. 2b that the permittivity $\varepsilon' \approx 17$ and conductivity σ (on the order of 10^{-9} $(\Omega\cdot\text{cm})^{-1}$) are constant in the temperature interval 5–160 K. According to Fig. 2a, there is a polar order along this axis in GMO at these temperatures. Beginning from $T \approx 160$ K slight growth in ε' and σ begin (Fig. 2b).

2.2. $Gd_{0.8}Ce_{0.2}Mn_2O_5$. Fig. 3a indicates that the significantly higher I_{pyro} and P along the c-axis occur in GCMO as compared to GMO in polarized field $E = 3.9$ kV/cm at $T < 160$ K. This switchable polarization practically is absent at $E = 0$. A comparison of Figs. 3a and 2a shows that low-temperature I_{pyro} anomaly (near 30–40 K) along the c-axis in GCMO is shifted to the higher temperature and it is significantly weakened in comparison with GMO. It indicates that

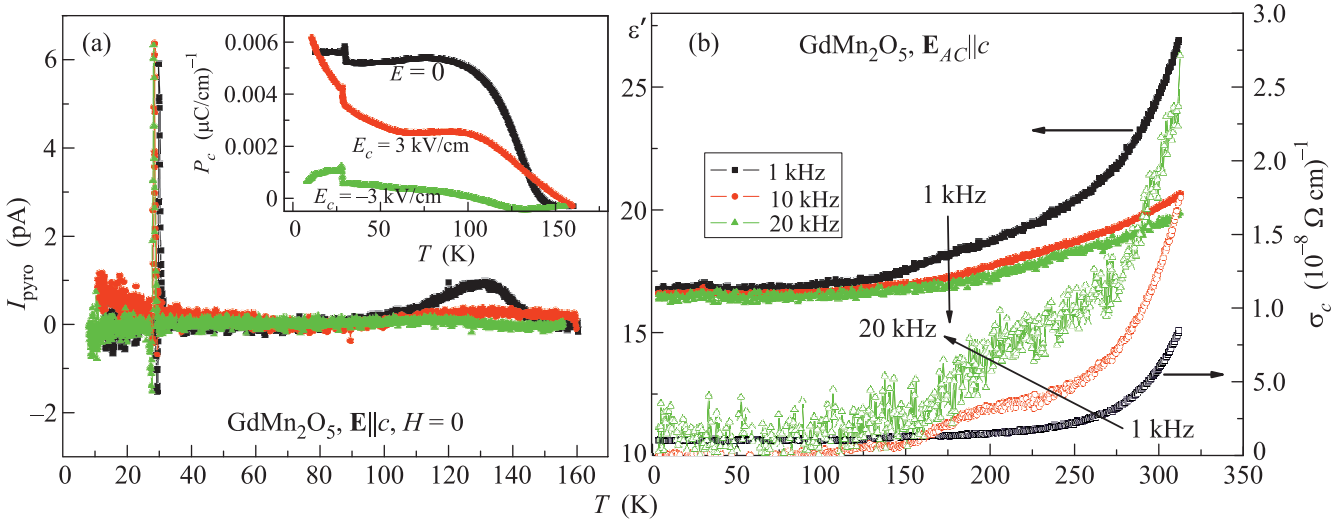

Fig. 2. Temperature dependences of I_{pyro} and P (inset) (a) and dielectric permittivity ε' (left axis, filled points) and conductivity σ (right axis, open points) (b) along the c-axis for GMO

the low-temperature charge distribution of Mn^{3+} and Mn^{4+} ions along the c-axis in GCMO is changed.

Fig. 3b demonstrates $\varepsilon'(T)$ and $\sigma(T)$ dependences along the c-axis in GCMO for the set of frequencies. The permittivity $\varepsilon' \approx 70$ and σ (on the order of $10^{-9}\,(\Omega\cdot\text{cm})^{-1}$) are seen to be constant in the temperature interval 5–160 K and 5–80 K, respectively. According to Fig. 3a there is a polar order along the c-axis at $T \le T_{C1} \approx 160$ K. There are two important facts that the σ growth is precursor of the polar state emerging and the $\varepsilon'(T)$ maximum which is typical of the ferroelectric structural phase transition is not observed near T_{C1}.

There is a dispersion in the conductivity: the higher the frequency, the higher the conductivity. The observed frequency dispersion of conductivity is typical of inhomogeneous systems containing domains of different sizes of localized charge carriers with electron correlations [15]. The percolation conductivity σ_{dc} has no frequency dispersion. The σ_{ac} with frequency dispersion characterizes local conductivities of restricted domains. The local conductivity can be defined as $\sigma_{\text{loc}} = (\sigma_{ac} - \sigma_{dc})/\sigma_{dc}$. There are three temperature intervals of the local conductivity dispersion, which are observed near 60, 150, and 250 K (see also Fig. 3c). In Figs. 3b and c the temperature ranges of local conductivity are separated by ones with weakened dispersion, especially between the second and third ranges. That points to the growth of percolation conductivity in these separated ranges. Fig. 3b shows also that there is dispersion in the permittivity values and temperatures of their step-like anomalies at $T > 160$ K. The higher the frequency, the lower the permittivity and the higher the temperatures of these anomalies. Such a dispersion shows that the dynamic restricted polar domains of different sizes coexist in GCMO at these temperatures. Thus, the polar order state at $T \le T_{C1} = 160$ K is transformed into the dynamic state with restricted polar domains of different sizes which is typical of the diffuse ferroelectric phase transition [16].

We suppose that anomalies in $\varepsilon'(T)$ occur if condition $\omega\tau = 1$ is met for restricted polar domains (ω is the circular frequency, $\tau(T)$ is the temperature-dependent polar domain lifetime). The Arrhenius law $\tau = \tau_0 \exp(E_A/kT_{\max})$ is fulfilled for these anomalies that allow one to estimate the activation barrier $E_A \approx 375$ meV that defines the characteristic energy of interaction in the state in which restricted polar domains coexist. Note that E_A corresponds by the order of magnitude to the double exchange that characterizes the charge transfer between manganese ions of different valences [5]. Fig. 3c shows that the first two low temperature ranges of local conductivity are free of maxima temperatures dispersion but they are dispersion in the magnitudes of local conductivity maxima, the higher the frequency, the higher the local conductivity. It is important that the temperature ranges of the local conductivity maxima and that of I_{pyro_c} maximum near 160 K coincide (see Fig. 3a). This means that the polar order near 160 K occurs in the crystal matrix consisted of the static domains with different sizes which are organized in the ordered state. Such type polar order can be assigned to the formation of 2D superstructure along the c-axis which involves the layers of different width con-

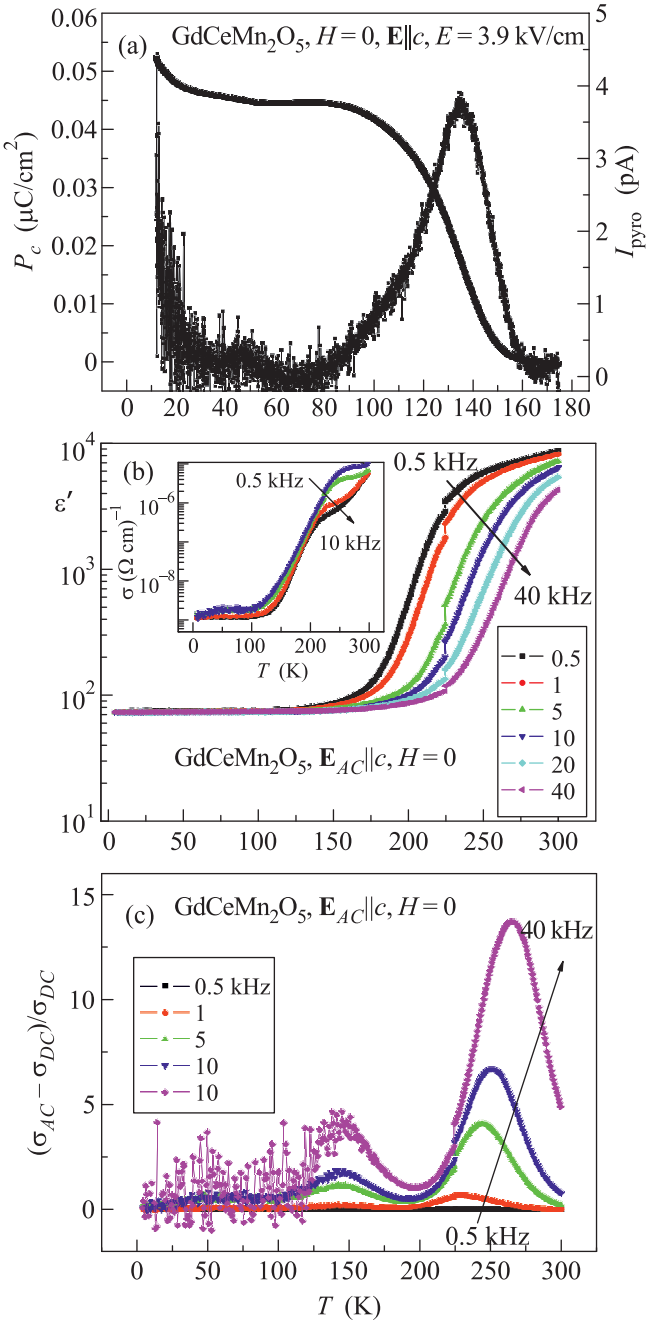

Fig. 3. Temperature dependences of the I_{pyro} (the right axis) and P (the left axis) (a), permittivities and conductivities (inset) (b), and local conductivities (c) along the c-axis. Figs. 3b and c are presented for set of frequencies indicated on these figures

taining the various quantity of Mn^{3+}–Mn^{4+} ion pairs. This periodical charge disproportion of the 2D superstructure is responsible for the polar order. In that case the polar phase transition may not be accompanied by the change of crystal symmetry. That is why, the permittivity maximum is typical of the ferroelectric structural phase transition is not observed in GCMO near 160 K.

Since the percolation conductivity grows in the temperature range 170–200 K, the leakage current grows at these temperatures as well. This prevents the I_{pyro} study at $T > 200$ K in GCMO. It appears reasonable that dynamically equilibrated 2D superstructures are still being formed at these temperatures but they become reconstructed due to the accumulation of additional electrons appeared at 170 K $< T <$ 200 K.

According to Figs. 3b and c the additional free of dispersion jumps of ε' and σ are observed at $T = 225$ K. Such type anomalies point to the lock-in type phase transformation. We attribute this lock-in transition to the new 2D superstructure formation near 225 K. Such superstructure is bound to consist of layers with enlarged concentrations of electrons and Mn^{3+} ions. With temperature growth the permittivity and local conductivity frequency dispersions are weakened as the $T \approx$ ≈ 300 K is approached (Fig. 3b). This means that correlations inside the superstructure layers begin to destroy due to the transformation of the some localized charge carriers into the percolation ones.

The 2D superstructure in GCMO is confirmed in X-ray diffraction studies which are performed for several samples of GCMO at room temperature (when the high-temperature 2D superstructure still exists, Fig. 3b). The angular intensity distribution of $\mathbf{(004)}_{CuK\alpha 1}$ Bragg reflections was detected in the 3-crystal regime with the Θ–2Θ scan having a resolution of $\approx 10''$. The half-width of the rocking curve (ω_Θ) for one of the Bragg peaks was measured in the (Θ-scan) regime, and the lattice constant d was inferred from the Bragg angle Θ_B of this peak. Fig. 4 shows diffraction curve for GCMO which

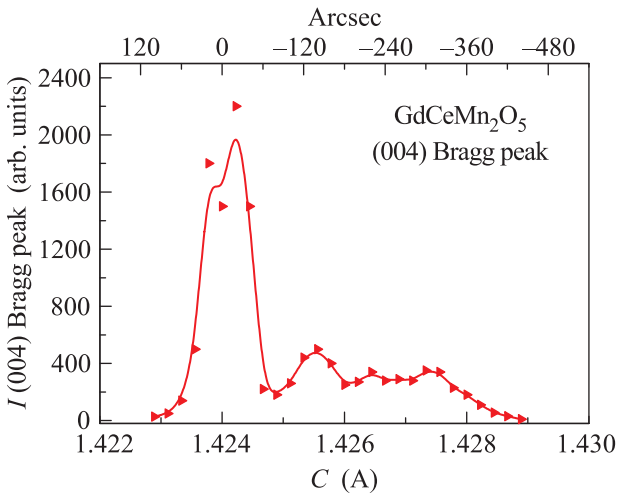

Fig. 4. Distribution of $\mathbf{(004)}_{CuK\alpha 1}$ Bragg reflection intensities for GCMO

exhibits a set of diffraction maxima whose positions are determined by parameter d and which characterize the layered crystal structure. The distances between the maxima $\Delta\Theta$ of these peaks give information on the lattice mismatch in the layers.

Let us consider the effect of magnetic field on the polar state and conductivity in GCMO. Fig. 5a presents

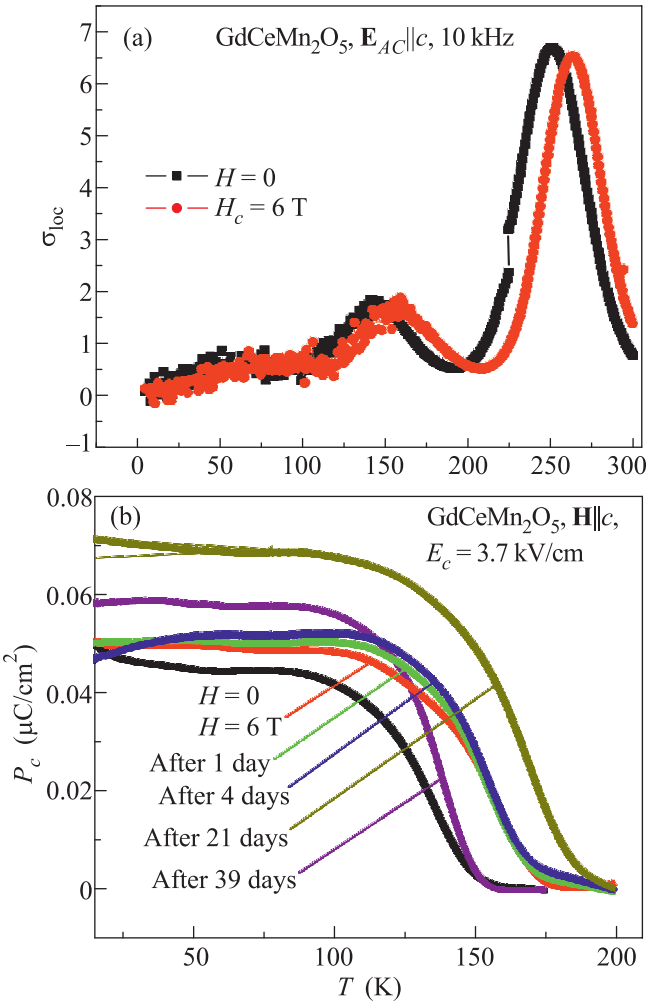

Fig. 5. A long-term after-effect of magnetic field on local conductivity (a) and P_c (b). $\mathbf{H} \parallel c$, $H = 6$ T

the effect of magnetic field on the local conductivity. It can be seen that the maxima of local conductivities are shifted to higher temperatures. In this case the lock-in phase transformation near 225 K is absent. Fig. 5b presents the effect of magnetic field on polarization P_c. It is evident that magnetic field $H = 6$ T leads to a growth both in polarization value and in temperature of P_c emergence. After magnetic field is switch off and the sample is heated to 300 K, repeated measurements of P_c by the same method but in zero magnetic field show a long-term after-effect of magnetic field. To restore the initial polarization (prior to application of H), many days are needed. We observed an irreversible effect of magnetic field on dielectric permittivity and conductivity in ECMO [8, 9] and $TbBiMnO_3$ [17].

We believe that magnetic field $\mathbf{H} \parallel c$ increases the double exchange between manganese ions with variable valences. This deepens the barriers at the boundaries of the restricted domains caused by phase separation. Indeed, the activation barrier E_A for the high-temperature step-like permittivity anomalies in magnetic field $H = 6$ T becomes 450 meV. As a result, the 2D superstructures formed due to the phase separation are characterized by the larger polarization and its retransformations are shifted to higher temperatures. This fact demonstrates the strong magneto-electric interaction at all temperatures but the long-term after-effect of magnetic field on polar states occurs.

Let us turn now to the low temperature polar state. As noted above the polar order along the b-axis emerges at $T \le T_C = 30$ K. Thus, at $T < 30$ K the polar domains with the perpendicular polarizations (along the b- and c-axes) emerge. As a result, the jumps in the internal electric field should occur near the domain walls separating these domains. This is energetically unfavorable. The domains and domain walls of such a type can exist if these internal fields are screened by charge carriers [18, 19]. The domain walls become charged. In our case it is due to availability of the local conductivity.

Our previous studies of the microwave magnetic dynamics of the set of RMO crystals (both initial and diluted ones) with different R ions (including GMO) were revealed the similar sets of ferromagnetic resonances which we attributed to the responses of individual 1D superlattice layers. We supposed that the 1D superlattices having the complex layered structure were charged domain walls between bulk multiferroic domains [20–22].

3. Conclusion. The temperature evolution of the polar states was studied in GMO and GCMO. Along with the abnormally high polarization which occurs in GMO along the b-axis at $T \le T_C = 30$ K the additional polar order along the c-axis at $T \le T_{C1} = 160$ K in both GMO and GCMO was revealed. In GCMO this polar order is on order magnitude larger than in GMO. The polar order near 160 K is induced by charge disproportion inside the 2D superstructure layers which are formed due to the phase separation and charge carrier self-organization.

At $T > T_{C1}$ the polar order is transformed into the dynamic state in which the restricted polar domains of different sizes with local conductivities coexist. This polar state is characterized by the giant permittivity with

frequency dispersion. Two these features of the phase transition near 160 K are typical of the diffuse ferroelectric phase transition.

At the lowest temperatures two polar orders with both orientations along the b- and c-axes coexist. The domains with perpendicular polarizations are separated by charged domain walls which are the 1D superlattices studied by us earlier.

The presence of an abnormally high polarization along the b-axis in GMO as compared with other RMO is confirmed by us. It is found also that this unidirectional rigid polarization is induced by the internal field.

The long-term after-effect of magnetic field on polarization and the temperatures of the all 2D superstructure reformations emerge. Magnetic field increases these parameters.

The authors would like to thank N.V. Zaitzeva for X-ray phase analysis of the samples. The work was partly supported by the Presidium of RAS (Programme P-20) and the Government of RF (project # 14.B25.31.0025).

1. N. Hur, S. Park, P.A. Sharma, J. S. Ahn, S. Guba, and S.-W. Cheong, Nature (London) **429**, 392 (2004).
2. E. I. Golovenchits, N. V. Morozov, V. A. Sanina, and L. M. Sapozhnikova, Sov. Phys. Sol. St. **34**, 56 (1992).
3. Y. Noda, H. Kimura, M. Fukunaga, S. Kobayashi, I. Kagomiya, and K. Kohn, J. Phys.: Cond. Mat. **20**, 434206 (2008).
4. P. G. Radaelli and L. C. Chapon, J. Phys.: Cond. Mat. **20**, 434213 (2008).
5. L. P. Gor'kov, Phys. Usp. **41**, 589 (1998).
6. J. Van den Brink and D. I. Khomskii, J. Phys.: Cond. Mat. **20**, 434217 (2008).
7. M. Yu. Kagan and K. I. Kugel, Phys. Usp. **44**, 553 (2001).
8. V. A. Sanina, E. I. Golovenchits, V. G. Zalesskii, S. G. Lushnikov, M. P. Scheglov, S. N. Gvasaliya, A. Savvinov, R. S. Katiyar, H. Kawaji, and T. Atake, Phys. Rev. B **80**, 224401 (2009).
9. V. A. Sanina, E. I. Golovenchits, V. G. Zalesskii, and M. P. Scheglov, J. Phys.: Cond. Mat. **23**, 456003 (2011).
10. J. Lorenzana, J. C. Castellani, and C. D. Castro, Europhys. Lett. **57**, 704 (2002).
11. K. I. Kugel, A. L. Rakhmanov, A. O. Sboychakov, F. V. Kustmarsev, N. Poccia, and A. Bianconi, Supercond. Sci. Technol. **22**, 014007 (2009).
12. N. Lee, C. Vecchini, Y. J. Choi, L. C. Chapon, A. Bombardi, P. G. Radaelli, and S.-W. Cheong, Phys. Rev. Lett. **110**, 137203 (2013).
13. E. I. Golovenchits and V. A. Sanina, JETP Lett. **78**, 88 (2003).
14. E. I. Golovenchits and V. A. Sanina, J. Phys.: Cond. Mat. **16**, 4325 (2004).
15. A. R. Long, Adv. Phys. **31**, 587 (1982).
16. G. Smolensky, Ferroelectrics **53**, 129 (1984).
17. E. I. Golovenchits and V. A. Sanina, JETP Lett. **84**, 190 (2006).
18. M. Y. Gureev, A. K. Tagantsev, and N. Setter, Phys. Rev. B **83**, 184104 (2011).
19. T. Sluka, A. K. Tagantsev, D. Damjanovich, M. Gureev, and N. Setter, Nature Comm. **3**, 748 (2012).
20. E. I. Golovenchits, V. A. Sanina, and V. G. Zalesskii, JETP Lett. **95**, 386 (2012).
21. V. A. Sanina, E. I. Golovenchits, and V. G. Zalesskii, J. Phys.: Cond. Mat. **24**, 346002 (2012).
22. V. A. Sanina, E. I. Golovenchits, V. G. Zalesskii, and B. Kh. Khannanov, J. Phys.: Cond. Mat. **25**, (2013).